

The Reactive Element Effect



KLAUS FRITSCHER

Rationalizing the reactive element effect operative in alumina- and chromia-forming alloys upon oxidation under oxidizing hot gas atmospheres, referring to investigations on zirconium oxide-coated test samples for gas turbine alloys. This retrospective study uses the results of cyclic furnace lifetime tests conducted at 1100 °C on ZrO₂-coated Ni-base alloys with Y- or Y+ Hf-doped bond coats and correlates them with the parabolic oxidation rate constant at 1100 °C of binary NiAl alloys doped with Y, Zr, or Hf. Parallel results at higher temperatures allow the respective oxidation processes during the cyclic lifetimes to be assigned to cation-dominated or anion-dominated transport processes.

The correlations document the close interrelationship between

- the refractory element content (Mo, Re, Ta, W) in the substrate alloy
- the total content of the two reactive elements Y and Zr in the mixed zone of the scale, representing a Me³⁺ iso-valence value
- individual relative lifetime parameters in pct for EBPVD thermal barrier coating systems associated with cation-dominated transport processes.

<https://doi.org/10.1007/s11661-022-06840-w>

© The Author(s) 2022

I. INTRODUCTION

A. The Reactive Element Effect: Phenomenology and Interpretative Approach

AS early as 1937, Pfeil *et al.*^[1] at first recognized that small additions of rare-earth elements like Y, Sc, Ce, and the lanthanides to Cr₂O₃-forming alloys (later also for Al₂O₃-forming alloys) cause a significant improvement in their oxidation resistance. Rare-earth metal addition as melt deoxidant to Nichrome (Ni-20Cr wt pct Cr) heating element was found to substantially increase its cyclic lifetime by increasing the adhesion of its surface Cr₂O₃ scale. The amount of the rare-earth additions must be kept low, to 0.01–0.5 wt pct.

A comprehensive retrospect of Whittle and Stringer^[2] realized that almost all elements that have a higher affinity for oxygen than the oxide layer-forming element, namely Cr and Al, showed this effect. They called it the reactive element effect. They examined the various positive effects of reactive elements on the performance and oxidation resistance of high chromium or aluminum alloys and alloy layers, respectively, of the

iron–platinum group—Fe, Ni, Co, Pt, Os, Ir—at high operating temperatures.

The reactive element effect was first summarized for chromia-forming alloys as follows:

1. Significant decrease of the parabolic oxidation rate constant.
2. Improved adhesive strength of the oxide layers.
3. Enhanced selective oxidation of chromium in the alloys sufficient for the formation of the protective layers.
4. Change of the scale growth mechanism from predominantly cation outward to oxygen inward mass transport.

All four effects also apply to Al₂O₃ formers, except that the manifestation of point 4 is different due to the fact that steady-state Al₂O₃ growth is already dominated by oxygen inward transport; reactive element additions reduce the cation outward transport, but do not alter the overall transport direction.

Various foremost mechanical models were put forward to explain the reactive element effect.^[2] The popular mechanisms (pegging, growth stresses, scale placidity, vacancy sink, chemical bond) were each addressed by simple logic tests to account for first-order effects on adhesion. The chemical bond explanations survived these tests. They relate to the chemical change that occurs at the scale/alloy interface when reactive elements are present. This can be a reduction in the

KLAUS FRITSCHER is with the DLR German Aerospace Center, 51107, Cologne, Germany. Contact e-mail: klaus.fritscher@goetttersiedlung.de
Manuscript submitted February 12, 2022; accepted September 18, 2022.

Article published online October 31, 2022

interface concentration of sulfur and the presence of reactive elements at the interface. The anticipated mechanism that relates to sulfur segregation is commonly referred to as the “sulfur effect.” Reactive elements also segregate and strengthen the scale/metal interface, while, at the same time and more importantly, they prevent ominous sulfur interfacial segregation by tying it up owing to their strong sulfide forming capability. For example, innovative Ni-base superalloys for turbine blades are additionally optimized (0.1 ppmw S) using the process engineering method of melt desulfurization under a hydrogen atmosphere.^[3]

Analogous to the example given of rigorous control of sulfur levels in Al₂O₃-forming Ni-base alloys, most of current research on the reactive element effect is about optimizing its beneficial effects. Results have consistently shown that lifetime (*alias* scale adhesion) is affected by the type and amount of reactive elements in a given type of alloy. However, quantitative information does not yet exist to allow accurate selections for optimization. Over-doping of reactive elements produces detrimental effects, in that the oxidation rate is increased and the scale adhesion decreased. Excess reactive elements in the alloy can form a second phase oxide or intermetallic compound with Al. They allow for fast oxygen transport, thus increase the scale thickness and can promote internal oxidation. They cause premature failure of the protective oxide layers. The process-related oxygen content in plasma-sprayed oxidation-protective coatings and bond coats likewise causes the precipitation of reactive element oxides, which limit the full potential of increased scale adhesion of the reactive elements present.

A selection of the questions for future research on the reactive element is listed below:

- The mechanism by which reactive elements retard cation but not anion grain boundary transport is unclear.
- The relative effectiveness of reactive elements varies in different types of alloys and cannot yet be explained.
- In more complicated commercial alloys and coatings, where numerous alloying elements are present, it is not known what synergism exists between these elements and the added reactive element.
- Co-doping of reactive elements has been shown to further improve alloy performance, but more work is needed to understand why.^[4]

A different approach based on physico-chemical evidences was chosen in this paper to understand the reactive element effect: The effects listed above point to material properties which, in the atomistic sense, include both a minimization of ionic mass transport *via* lattice defects and a maximization of binding forces between anions and cations. The interrelationship of both mechanisms is discussed in the following.

In particular, this paper addresses the following:

the ionic bond in Al₂O₃ and Cr₂O₃ within the oxides growing at high temperatures,

the parabolic oxidation rate constants at high temperature resulting from the transport mechanism *via* lattice defects in the oxide and their oxygen pressure-dependent defect concentration,

the adhesive strength as a measure of the FCT (cyclic furnace test) lifetime of TBC (thermal barrier coating) samples, the FCT test process and its relation to the activation energy for identifying cation- and anion-dominated mass transport,

influence of tetravalent foreign cations stemming from the base alloy on the lattice defect concentration-dependent lifetime of TBC samples, and

influence of monovalent foreign cations on the change in the scale growth mechanism from predominant outward to inward mass transport.

II. THE DOMINANT TYPE OF BOND IN THE OXIDES ON REACTIVE ELEMENT-DOPED ALLOYS

The electro-negativities of the elements involved in compounds as proposed by Linus Pauling articulate the type of covalent chemical bonds formed when atoms share electrons. The Pauling values are between 0.7 (Francium) and 4 (Fluorine). The Pauling values for aluminum and oxygen are 1.61 and 3.44. The amount of the difference, the ion-binding difference, is a decisive feature for the stability of the bond between elements of a compound. The ion-binding difference is easy to determine because only two elements aluminum and oxygen are involved. It is 1.83. The ionic binding difference between oxygen and chromium shows a slightly lower value of 1.78.

The corresponding threshold value for the distinction between ionic bond (heteropolar bond) and covalent bond is anticipated to be around 1.7. Accordingly, the prevalent ionic bonding is likely to be with Al₂O₃ and Cr₂O₃. The comparison value for Fe₂O₃ (hematite), for example, is 1.61. Accordingly, although hematite represents the same corundum structure as Al₂O₃ and Cr₂O₃, the type of bond in hematite is based on the (weaker) covalent bond.

The following reflections of transport mechanisms *via* ions and vacancies in identical crystal structures show that positioning of cations at interstitial sites in the crystal lattice of a covalent-bound oxide is typical, whereas no interstitial cations are allowed in the ionic (heteropolar bound) crystals. Instead, cation and oxygen vacancies are generated there.

III. THE INHERENT MECHANISMS OF MASS TRANSPORT

The prerequisite for ionic mass transport is the presence of crystal defects. These are point defects in the matter of interstitial ions and ion vacancies. They allow the growth of oxide layers on their metal substrates.

The concentration of the various point defects are controlled by point defect equilibria. These concentrations are clearly defined for the respective individual crystal structure when the temperature, pressure, and chemical potentials alias activities of the components are given. When the values for temperature and pressure are given, for simple oxides such as Al_2O_3 it is sufficient to state only one component activity, conveniently the oxygen activity given in atmospheres atm.

The thermodynamic analysis allows the following statement on the basis of the point defect equilibria; they refer to a characteristic dependency between the mole fractions of the defects and the oxygen activity: If the defect equilibrium is dominated by only one type of point defects—interstitials or vacancies—over a larger oxygen activity range, there is a linear relationship between the logarithms of the concentration of these point defects and the oxygen activity.

In this way, it can be determined whether a Frenkel-type or Schottky-type thermal disorder exists. Frenkel-type disorder enables mass transport according to an interstitial mechanism. Schottky-type disorder empowers mass transport according to the vacancy mechanism.^[5]

IV. REFRESHING TRANSPORT MECHANISMS: FRENKEL VS SCHOTTKY

The dominant point defects in a Frenkel-type crystal are cation vacancies and interstitial cations. They arise when a cation leaves its regular lattice position (a fixed position in the lattice) and takes an unoccupied position in the intermediate lattice; and it can be set aside again in reverse order. In Kröger–Vink notation, the interrelationship of cation positions at orderly and interstitial lattice sites can be described as follows: $(\text{Me}_{\text{Al}}^{3+})^X + (V_{\text{Al}}^{\circ\circ})^X \rightleftharpoons (\text{Me}_{\text{iAl}}^{3+}) + (V_{\text{Me}}^{\circ\circ})$. The superscript X indicates a fixed position in the lattice. The subscript iAl refers to a transient interstitial position in the cation lattice.

Interstitial cations thereby yield a continuous decrease of the concentration of point defects with increasing oxygen activity. The ionic mass transport thus decreases correspondingly with the decreasing concentration of point defects *alias* the increasing oxygen potential. This case of a Frenkel-type disorder is met by hematite, for example.^[6]

The characteristic point defects in a Schottky-type crystal are cation vacancies and oxygen vacancies. The point defects are created by the transfer of an oxide molecule from the crystal into the gas phase. In Kröger–Vink notation, the interrelationship of cation and anion sites can be expressed as follows: $2(\text{Me}_{\text{Al}}^{3+})^X + 3(\text{O}_{\text{O}}^{2-})^X \rightleftharpoons (V_{\text{Al}}^{\circ\circ}) + 3(V_{\text{O}}^{\circ}) + \text{Al}_2\text{O}_3$ (gas molecule).

It should already be mentioned at this point that additional point defects can be generated in the alumina crystal by incorporating lower-valued cations of the type Me^{1+} or higher-valued cations of the type Me^{4+} . The

presence of these “foreign elements” in the oxide crystal lattice is due to the individual composition of the oxidizing base alloys. Their impact has to be taken into account in order to meet the conditions of electrical neutrality. The site ratio for cations, anions, and vacancies in their sub-lattices is given by

$$(\text{M}_{\text{Al}} + V_{\text{Al}}^{\circ\circ}) : (\text{X}_{\text{O}} + V_{\text{O}}^{\circ}) = 2 : 3. \quad [1]$$

If only one type of thermal disorder namely either cation vacancies or oxygen vacancies dominates the transport behavior in a large oxygen activity range *alias* oxygen pressure range Δp_{O_2} , then, depending on the type of disorder, characteristic oxygen activity dependencies result for the ranges of the mass transport dominating point defects.

The oxygen pressure dependency of the point defect concentration of $V_{\text{Al}}^{\circ\circ}$ referring to cation-dominated outward mass transport in Al_2O_3 is as follows:

$$\partial \log [V_{\text{Al}}^{\circ\circ}] / \partial \log p_{\text{O}_2} = 3/16. \quad [2]$$

Interestingly, the same oxygen pressure dependency also corresponds to the self-diffusion coefficient of triply charged vacancies $V_{\text{Cr}}^{\circ\circ\circ}$ in single crystal Cr_2O_3 between 1490 and 1570 °C, where the required oxygen partial pressures were set by using CO/CO_2 gas mixtures.^[7]

In a subsequent, even deeper low p_{O_2} regime anion vacancies V_{O}° will be governing the oxidation processes. The oxygen pressure dependency of the point defect concentration of V_{O}° for anion-dominated inward mass transport is as follows:

$$\partial \log [V_{\text{O}}^{\circ}] / \partial \log p_{\text{O}_2} = -1/6. \quad [3]$$

These theoretical values of the oxygen pressure dependence of the point vacancy concentration correlate to trivalent cations Me^{3+} and divalent anions O^{2-} with reference to point vacancy thermodynamics. If the oxidation of protective layer-forming alloys is based on parabolic scale growth rates, it makes sense to compare the theoretical dependencies with real kinetic data on scale growth. The data can be recorded either as the increase in the thickness of scales or their increase in weight *vs* time at constant temperature. The oxidation curves generated by thickness measurements or *via* thermo-gravimetry provide appropriate comparison standards in terms of “parabolic oxidation rate constants” often listed in open literature, for example, in $\text{g}^2 \text{cm}^{-4} \text{s}^{-1}$. The parabolic oxidation rate constants are proportional to the ionic mass transport. They are shown for alumina-forming “binary” NiAl alloys (each un-doped or RE-doped) at 1100 °C in dependence of their respective oxygen activity range in Figure 1.

The data in Figure 1 show a substantial decrease of the parabolic oxidation rate constants at decreasing oxygen activities. The tendency towards reduced parabolic oxidation rate constants is due to the oxygen pressure-related decrease in the concentration of point defects in the crystal lattice. The decrease of p_{O_2}

according to 3/16 represents the diffusion of cation vacancies.

This tendency corresponds to the contribution of the reactive elements. The oxidation of the Y-, Zr-, and Hf-doped alloys show different oxidation rates, the related activation energies, however, display a uniform value of 370 to 382 kJ mol⁻¹ for the Y- and Zr-doped alloys. They represent the dominating diffusion of cation vacancies. In contrast, the Hf-doped alloy displays a higher value of around 500 kJ mol⁻¹. In this case the activation energy is determined by the diffusion of the slower moving species. The diffusion is anion-controlled.

This significantly higher value indicates a change in the transport-dominant ion vacancies from cation to anion vacancies. The mobility of the respective ions, which are subjected to thermally activated jump processes, is crucial for the dominating type of cation or anion transport. A decrease of p_{O_2} according to 3/16 represents the diffusion of cation vacancies.

The dotted lines indicate the respective oxygen pressure range in which, according to 3/16, the outward-dominated mass transport *via* cation vacancies, and, according to -1/6, the inward-dominated mass transport *via* anion vacancies, predominates. They represent reference lines for the oxygen pressure ranges at the respective trend of increase and decrease of

related data. In the oxygen pressure range according to the specification - 1/6, the inward-dominated mass transport *via* oxygen vacancies prevails. The measured value for NiAl + 0.05Hf represents a single value for a specific p_{O_2} . In order to be able to clearly show the oxygen pressure dependency of - 1/6, an additional measuring point in the adjacent pressure range would make sense, but is not yet available.

The relationships between the relative concentrations of point defects (the related diffusion coefficients as well) as a function of the oxygen potential indicate the existence of a concentration minimum of point defects. This relevant oxygen pressure range is conceivable between about 10⁻²⁹ and 10⁻³⁶ atm in Figure 1.

Notably, the oxides of the 4th group elements hafnia and zirconia do not form compounds nor solid solutions with alumina; however, a certain solubility of oxygen in doped alloy substrates is likely. They will probably have an effect on the diffusion processes in the TGO at p_{O_2} pressures below those of the decomposition pressure of YAG (Al₅Y₃O₁₂) of 10⁻²⁸ atm. Consequently, the pressure for hafnia can be assumed to be ~ 10⁻³⁷ atm and that of zirconia between those of hafnia and YAG according to 10⁻³⁷ atm < p_{O_2} zirconia < 10⁻²⁸ atm at approximately 10⁻²⁹ atm. The exceptional high weight gain rate constant for the NiAl + Zr alloy compared to

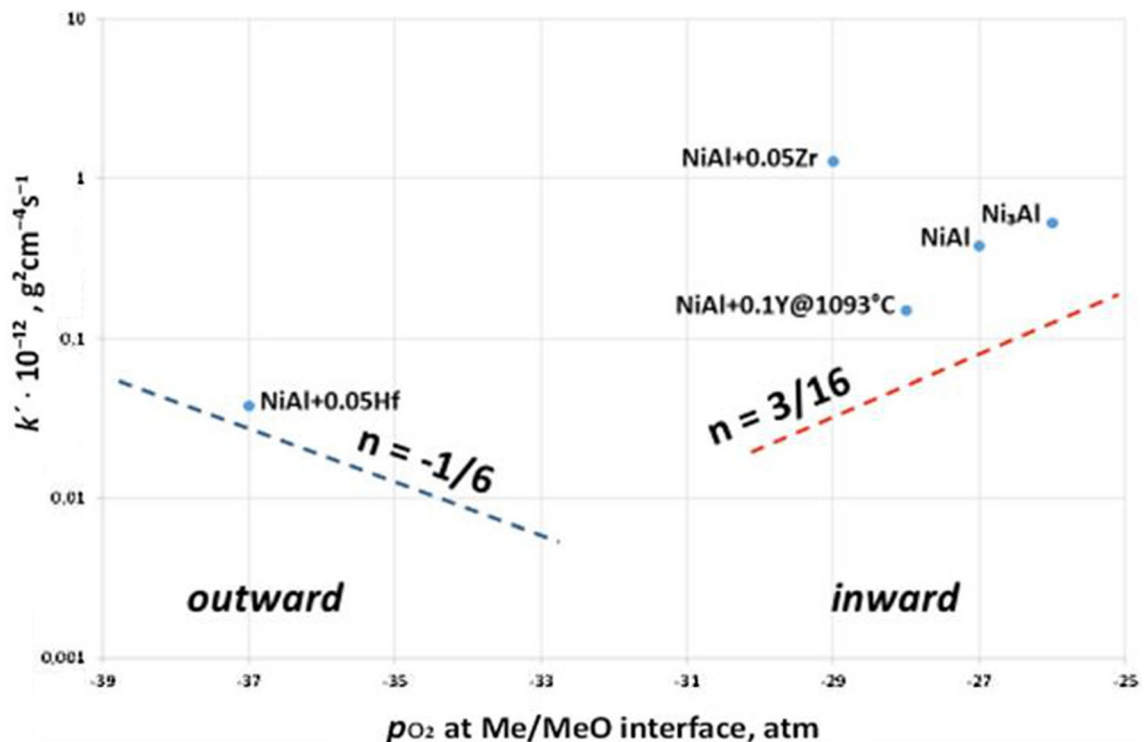


Fig. 1—Oxygen pressures at the growth front of alumina-forming “binary” NiAl alloys (each un-doped or RE-doped) at 1100 °C *vs* their respective gravimetric experimental parabolic oxidation rate constants of these alloys. The data of the parabolic oxidation rate constants, lined up from right to left, are taken from literature. When in doubt, the lowest possible RE values were used to balance the weight gain rate accelerating effect of over-doping. The oxidation tests of the alloys listed here have been carried out on polycrystalline material in different laboratories and institutes; the grain size in the various scales, however, which certainly have an influence on the scale growth rate according to the density of the grain boundaries in the scale, have not been discussed in this study. The slope n of the dotted lines indicates the oxygen pressure dependency *vs* the parabolic oxidation rate constants $\partial \log [V_{Al}^{vac}] / \partial \log p_{O_2}$ and $\partial \log [V_o^{vac}] / \partial \log p_{O_2}$ according to Eqs. [2] and [3]. Rate constants are given for Ni₃Al,^[19] NiAl,^[10] NiAl + 0.1at pct Y at 1093 °C,^[20] which each refer to a p_{O_2} according,^[21,22] NiAl + 0.05at pct Zr,^[23] and NiAl + 0.05 at pct Hf^[14] given at 10⁻³⁷ atm.^[24] Adapted from Ref. [12] under the terms of the CC BY license.

the neighboring NiAl + Y alloy is due to additional weight gain as a result of oxygen intake dissolved in the Zr-doped NiAl metal matrix. It is therefore reasonable to assume that the decisive rate in thickness growth of Zr-doped NiAl is lower than that of the neighboring Y-doped NiAl. The weight of the scale is reported to be one-tenth of the total oxidative weight gain.^[8]

V. SERVICE LIFE OF ZIRCONIUM OXIDE-COATED RENÉ 5 SUPER ALLOY TEST SAMPLES

In this section, the findings on lifetimes of NiCo-CrAlY bond-coated thermal barrier coatings applied to substrate samples of a turbine blade alloy are reviewed, which have been achieved under various cyclic thermal fatigue tests.

The failure times of NiCoCrAlY thermal barrier-coated René 5 substrates (Ni-7Cr-7.5Co-1.5Mo-5W-6.2Al-6.5Ta-3Re in wt pct) were determined by means of various FCT (cyclic furnace testing) programs, the cycles of which had different dwell times at high temperatures. The substrates had been coated by industrial partners *via* argon shrouded or detonation gun PS processes of NiCoCrAlY bond coats and EBPVD YSZ ceramic top coats. The nominal composition of the bond coats is Ni-22Co-16Cr-13Al-0.05Y in wt pct.^[9] In addition to the influence of the different production lines by the suppliers, the influences of different FCT routines on the failure times were statistically evaluated. The samples failed for the most part by spallation of the TGO along the bond coat/oxide interface with numerous crack excursions and oxide protrusions that extended into the bond coat due to reactive element oxide particles. Despite a wide range of results of the failure times, certain tendencies could be identified. A key message from this test campaign is the failure times of NiCoCrAlY bond-coated René 5 samples with EBPVD YSZ top coats follow an Arrhenius-type relationship with an activation energy of failure times of 356 kJ mol⁻¹. This value for the samples—having 16 pct Cr in their bond coats—is close to that obtained from the parabolic rate constants for the growth of α -Al₂O₃ scales. The value fits in sufficiently well with the activation energies of the parabolic oxidation rate constants for NiAl (382 kJ mol⁻¹) and NiAl-34 pct Cr (343 kJ mol⁻¹) shown in Figure 2. It presents a new way of determining the activation energy for oxide growth in thermal barrier coating systems.

VI. EFFECT OF INCORPORATING EQUIVALENT CR CATIONS IN THE LATTICE OF α -AL₂O₃ ON THE PARABOLIC OXIDE GROWTH RATE AND THE ACTIVATION ENERGY OF OXIDE GROWTH

As a result of the uptake of Cr cations Cr³⁺ at the original positions of the Al³⁺ ions, both an acceleration of the parabolic oxide growth rate and a reduction in the activation energy of the oxide growth^[10] are shown in

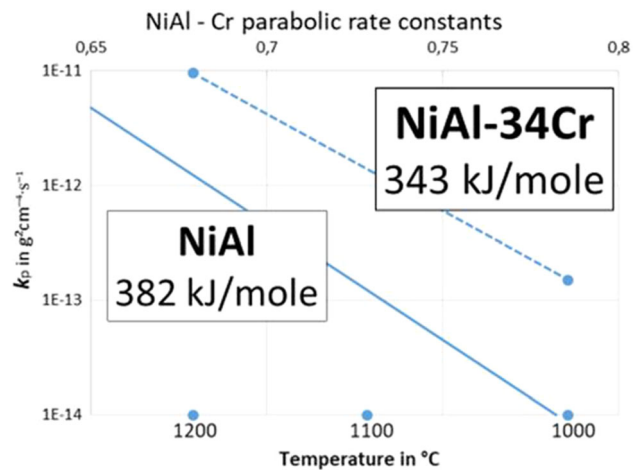


Fig. 2—Arrhenius plot, showing the parabolic oxidation rate constants k_p for un-doped NiAl^[10] and for NiAl-34Cr at 1000 to 1200 °C acc. data from Brumm *et al.*^[10] They deliver the appropriate activation energies for the transport of cations of 382 kJ mol⁻¹ and of 343 kJ mol⁻¹ in the Schottky-type crystal lattices of α -alumina representing cation-dominated outward transport *via* counter-diffusing Al vacancies.

Figure 2. The higher oxidation rates of Cr-alloyed NiAl alloys are not caused by a higher concentration of cation vacancies but by the Cr cation self-diffusion in α -Al₂O₃, where Cr³⁺ ions on the Al³⁺ ion sites are active. The diffusion characteristics of Al³⁺ and Cr³⁺ in alumina differ.^[11] Thus, the faster cation mobility of Cr³⁺ in α -Al₂O₃ accounts for both the faster TGO growth rates and lower activation energies of oxide growth.

VII. THE LIFETIMES OF VARIOUS TBC-COATED NI-BASE ALLOY SAMPLES ATTRIBUTABLE TO THE BINDING FORCES ARE COMPARED TO THE FCT-INDUCED MASS TRANSPORT

The failure times of thermal barrier-coated Ni-base alloys of different compositions without and with NiCoCrAlY bond coats were determined by means of identical FCT (cyclic furnace testing) programs. The NiCoCrAlY bond coats were fabricated exclusively in the laboratory at DLR using PVD (physical vapor deposition) processes.

The dependence of the service life of TBC samples was investigated with regard to the chemistry of the TGO formed on the Ni-base substrates.^[12] The standard NiCoCrAlY bond coat composition of the experimental campaign is Ni-21Co-19Cr-12Al-0.15Y in wt pct. The EBPVD process runs in a high vacuum atmosphere. PVD methods of deposition of bond coats in a vacuum atmosphere avoid the precipitation of harmful oxide particles of reactive elements and ensure the formation of a homogeneous and reproducible layer. Strict control of the content of reactive elements is particularly noteworthy. Over-doping of reactive elements produces detrimental effects, as they cause premature failure of the protective scales. In the current case mentioned above, for example, an optimal value of 0.15 wt pct Y

has been determined experimentally, which must not be exceeded.

The subsequent deposition of ceramic YSZ top coats in a low-pressure reactive atmosphere *via* reactive EBPVD processing supports the formation of a mixed zone (MZ) interlayer containing alumina, along with zirconia and yttria. This experimental approach opens up a way of decoding the reactive element effect for alumina-forming alloys.

The advantage of PVD bond coats is related to the absence of oxide inclusions, which cannot be ruled out in plasma-sprayed bond coats due to the typical internal oxygen content. Hence, the resulting PVD-coated samples should show highly reproducible specific service lives at temperature and failure appearance.

The details for the good reproducibility of the results on the EBPVD-coated samples are as follows:

1. The YSZ ceramic vapor cloud condensing on the bond coat interacts with the oxidizing alumina-forming metal surface in a hot reactive gas atmosphere; the outward growing transient Al sub-oxides (γ -, θ -Al₂O₃, spinels) mix with the YSZ condensate to form a so-called “mixed zone” intermediate layer. In the course of the vapor deposition process, the transient Al oxides start to convert into stable α -Al₂O₃. Finally, a stable mixed zone that does not continue to grow is formed. Meanwhile, further oxide growth takes place at the bond coat/ α -alumina interface *via* inward-directed selective parabolic oxidation of Al. The now stable α -Al₂O₃ in the mixed zone is in thermodynamic equilibrium with the stable α -Al₂O₃ of the thermally growing oxide layer. However, the oxygen activities in the mixed zone at the oxide/atmosphere and at the oxide/bond coat phase boundaries are different. They are the primary driving force that activates the mass flow of ions through the cross-section of the TGO. The thermal energy in turn is responsible for the concentration and mobility of the ion vacancies.
2. Off-diffusion of cations such as Y and Cr is achieved *via* vacancies in the cation sub-lattice. They accumulate in and at the mixed zone. In addition, the mixed zone has the option of interacting with the YSZ topcoat if necessary. The incorporation of Y and Zr in the mixed zone originating from the YSZ top coat arises according to the thermodynamic requirements. It is to be expected that the amounts of elements accumulating in the mixed zone as a result of the various high temperature exposures will be reflected in the respective chemical composition of the mixed zone. They can be a measure for the performance *alias* adhesion of the oxide layers.

The standard EBPVD TBC systems fail at the end of life owing to Al and Y depletion below the TGO. In parallel, the concentration of Y + Zr has reached a service-life-determining value of 3.7 at pct for the relative life of 1 (*alias* 100 pct of service life) in the mixed zone (see Figure 3). In addition, pores are found

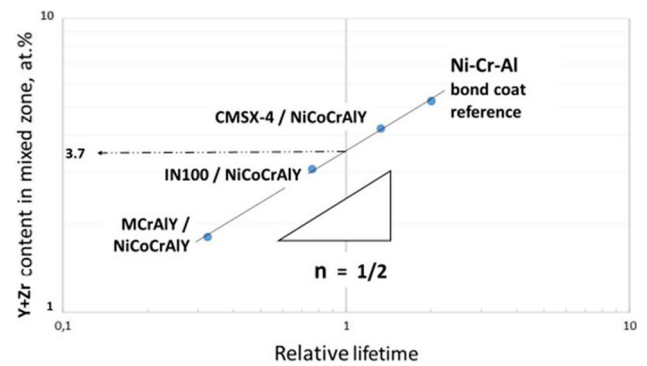


Fig. 3—Y + Zr content in at pct in the MZ *vs* relative lifetime on three different EBPVD NiCoCrAlY bond-coated TBC systems and an un-doped NiCrAl bond coat reference TBC system in log-log format. 100 pct of lifetime correlate with 3.7 at pct Y + Zr in the MZ.^[25] The “uniform lifetime relationship” also includes RE-free substrate TBC systems. Adapted from Ref. [25] under the terms of the CC BY license.

in the mixed zone. Their formation is probably due to the agglomeration of counter-diffusing oxygen vacancies.

The set of Ni, Co, Cr in the upper area of the TGO, whose oxides have a higher decomposition pressure for oxygen than alumina, are going to cause the formation of spinel phases below the TGO due to the thermodynamic equilibrium between the stable α -Al₂O₃ on both sides of the TGO layer. The total amount of Y + Zr represents a single “iso-valence value” for the two reactive elements Y and Zr.

This value represents a “gross” stoichiometric value of the two reactive elements. The element yttrium is in fact trivalent according to Y³⁺ and remains trivalent regardless of the oxygen partial pressure p_{O_2} . The element zirconium, on the other hand, is tetravalent according to Zr⁴⁺, but has a high solubility for oxygen in zirconium oxide according to ZrO_{2-x}. At low oxygen partial pressures, the oxygen content in zirconium oxide drops and approximates a stoichiometric composition of Zr₂O₃. This oxide has been described as being (Zr²⁺, Zr⁴⁺)(O²⁻, V_O^{oo})₂ according to a model in the zirconia lattice in combination with a high concentration of oxygen vacancies.^[13]

Y + Zr in the mixed zone is a life-predicting parameter for Ni-based EBPVD TBC systems. A parameter of < 3.7 pct indicates the proportion of the service life that is still available. In essence the MZ represents a chemical archive about the life of a TBC system.

VIII. COMPARING CYCLIC FURNACE TESTS (FCT) WITH A COMBINED THERMOMECHANICAL CYCLIC TEST OF A THERMAL BARRIER COATING SYSTEM

Figure 4 shows the result of the separation failure along the bond coat/TGO interface of an IN100 substrate-based thermal barrier system incorporating an EBPVD-manufactured bond coat by thermal fatigue due to FCT (cyclic furnace test) routines. (Composition

of IN100 substrate: Ni-base-14Co-9Cr-5Al-5Ti-2.3-Mo-1 V in wt pct.)

An equal thermal barrier system is presented in Figure 5. It includes an initial FCT application to form a TGO layer, followed by an additional superimposed thermomechanical treatment. The laboratory test aims to simulate extraordinary flight maneuvers of turbine aircraft including the influence of an FOD impact during the system's intermediate lifetime induced *via* a single harsh tensile cycle.

Figures 4 and 5 show the different progression of separation failure as a result of FCT (cyclic furnace testing) and thermomechanical fatigue testing on identical TBC systems. The additional mechanical loads resulted in a substantial reduced life of the sample and an untypical failure mode. The crack propagation as a result of the additional thermomechanical fatigue loads does not take place any more along the bond coat/TGO interface as typically expected only at the end of FCT lifetime for PVD-manufactured samples, but deviates into the weaker metallic bond coat. Potential crack propagation along the Me/TGO interface is definitely left out due to both the exclusion of the sulfur effect and the prevention of over-doping with reactive elements. As a result the bond coat/scale (TGO) interface remains stable. Even so the immediate vicinity of the bond coat benefits from the superior stability and adhesion of the metal/scale interface.

IX. EFFECT OF TETRAVALENT REFRACTORY ELEMENTS MO, RE, TA, W IN THE OXIDE LATTICE ON THE LIFE-DETERMINING Y + ZR CONTENT OF THE MIXED ZONE

In order to prevent confusion about the actual valences of the cations of the refractory elements on the bond coat side of the TGO in this chapter, it should be noted that some cations change their oxidation state as a function of the oxygen partial pressure. The bond coat side of the TGO is under reducing conditions, so it has a low p_{O_2} . The cations of the refractory elements mentioned at the beginning change their "ordinary" oxidation state by going to their lowest state according to thermodynamics to $4+$. Here they are tetravalent.

Point defect reactions in the lattice running at the bond coat side of the TGO most likely exert an effect on the defect concentration towards the exterior TGO including the alumina matrix of the MZ. Any increase in point defect concentration—caused by the refractory element solution-strengthened substrate—is balanced by the accumulation of reactive elements Y + Zr in the MZ thus matching thermodynamic equilibrium conditions.

The dynamics of the relationship between refractory element content in the substrates after 500 cycles *alias* 417 hot hours at 1100 °C *vs* the Y + Zr content in the MZ are demonstrated in Figure 6. The refractory element content of three substrates IN100 with 1.3 at pct, CMSX-4 with 5.5 at pct and MCrAlY with 0 at pct are given as examples. Although the cation vacancies are intended for the diffusion of trivalent cations like Al^{3+}

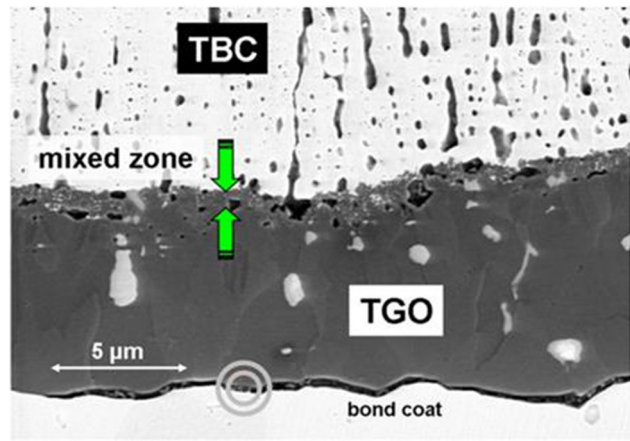


Fig. 4—Characteristic mixed zone (MZ) presented in a standard EB-PVD NiCoCrAlY bond-coated IN100 superalloy TBC system after FCT at 1100 °C showing typical separation failure at the Me/TGO interface at end of life; SEM micrograph, reprinted by personally granted permission of W. Braue.^[26] The 1.5-µm-thick MZ between YSZ TBC topcoat above and columnar TGO below is indicated by arrows. Early spinel phase located within the separation crack is marked by circles.

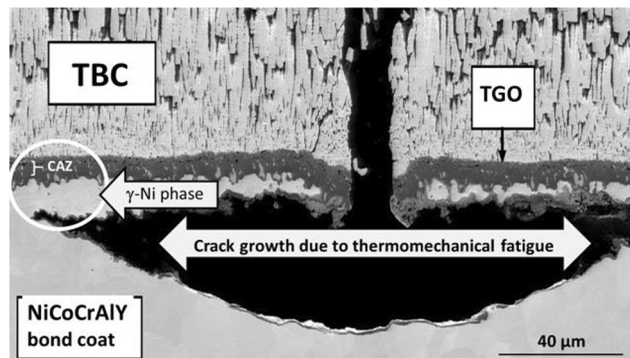


Fig. 5—End of life failure of a standard EB-PVD TBC material on IN100 superalloy substrate subjected to additional thermomechanical fatigue stresses *via* thermomechanical multiaxial fatigue testing. SEM micrograph, courtesy M. Bartsch^[27] adapted by permission of TTP. Crack propagation is restricted to the γ -Ni bond coat area (marked by a white circle) close below the Columnar Alumina Zone of the TGO representing both the weakest part in the bond coat and the superior cohesion of the Me/TGO interface within the layered structure of the system.

and Y^{3+} , as suggested in Eq. [1], they can also be used for the transport of the tetravalent refractory elements. For reasons of electro-neutrality, however, additional vacancies in the cation sub-lattice have to be created. So the diffusion rate of refractory elements in the TGO rises in proportion to the increasing concentration of cation vacancies.

The linear plot in Figure 6 confirms a square root relationship between Y + Zr content in the MZs after 417 hot hours and the refractory element content in at pct in the substrates. Although a standard distance through the bond coat of 100 µm had to be overcome, it thus gives an indirect evidence for the action of refractory elements on diffusion-controlled processes running between the substrate alloys and the MZ. The

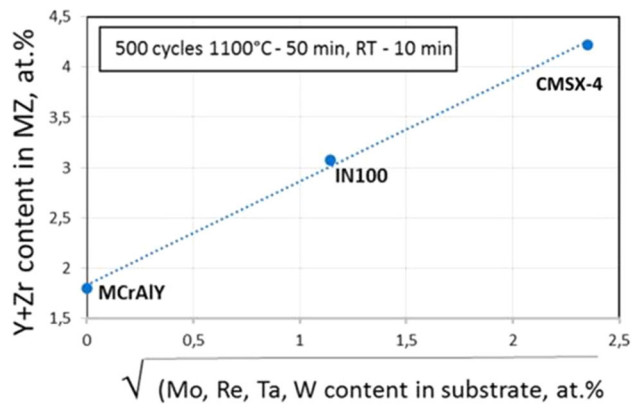


Fig. 6—Refractory element content (square root values) of YSZ top-coated Ni-base alloy vs Y + Zr content in the MZ after exposure to identical hot hours (417 h at 1100 °C). The straight line representing a square root relationship indicates outward diffusion-controlled transport of the refractory elements in dependence of the Y + Zr content in the MZ, in which the increasing Y + Zr concentration increases in proportion to the cation vacancy concentration. Reprinted from Ref. [28] under the terms of the CC BY license.

service life of TBCs becomes shorter, as the content of refractory alloys in the substrates increases.

The correlations document the close interrelationship between

- the refractory element content (Mo, Re, Ta, W) in the substrate alloy,
- the total content of the two reactive elements Y and Zr in the mixed zone, representing a Me^{3+} reactive element iso-valence value,
- relative lifetime parameters in pct of the EBPVD thermal barrier coating systems.

X. INFLUENCE OF THE DOPING OF THE SUBSTRATE ALLOYS OR BOND COATS WITH HF ON THE TYPE OF MASS TRANSPORT

Hf-alloyed super alloys René 142 (refractory element content of 4.74 at pct) and MarM002 (refractory element content of 1.35 at pct) with EBPVD standard NiCoCrAlY bond coats have been FCT short-term loaded for 1695 and 935 hot hours. Their mixed zones were analyzed, so to speak, in their middle period of life, the Y + Zr contents evaluated. A FCT series on CMSX-4 super alloy samples having an EBPVD with 0.2 at pct Hf-doped NiCoCrAlY bond coat showed an average lifetime of 4550 hot hours. An activation energy of lifetime of 474 kJ mol^{-1} was determined which is close to that of the parabolic oxidation rate constant for Hf-doped NiAl alloy of about 500 kJ mol^{-1} .^[14] This value is indicative for anion-ruled transport processes. Since the Hf contents in the substrate alloys as well as in the Hf-modified bond coats of the Hf-free substrate alloy lead to anion-dominated transport processes, a uniform lifetime of 4550 h at 1100 °C for all the Hf-alloyed alloys and for the substrate having an Hf-containing bond coat is anticipated. The

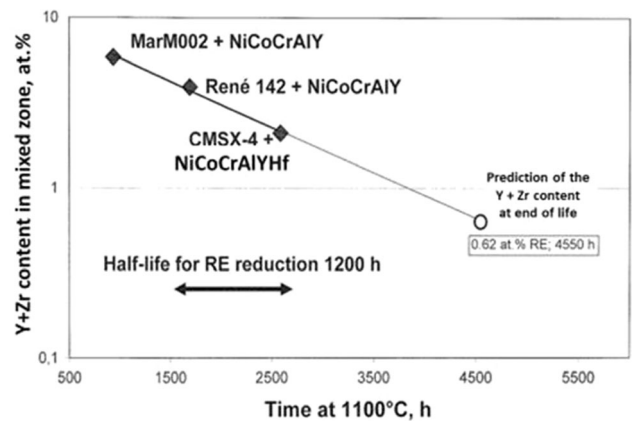


Fig. 7—Y + Zr content (at pct) in the mixed zone vs time at 1100 °C during FCT of Hf-holding TBC samples and Hf-modified bond-coated samples showing a logarithmic rate of Y + Zr reduction with time. The half-life value of 1200 h is calculated from the downtilt; it allows to estimate the RE content at FCT failure. Reprinted from Ref. [12] under the terms of the CC BY license.

cation-forming refractory elements in the substrates of 4.74 and 1.35 at pct have no longer any effect on the lifetime of the samples because their transport processes are now anion-dominated. The mixed zones after 935, 1695, and 2587 hot hours at 1100 °C were analyzed. The resultant Y + Zr contents in the mixed zone vs lifetime are shown in Figure 7.

The fine-grained mixed zone in Figure 8 is similar in size and microstructure to the “standard” mixed zone on Hf-free NiCoCrAlY bond coats which can be seen on a smaller scale in Figure 4. However, the TGO below is no longer single-phase columnar alumina matrix but poly-phase. The alumina matrix accommodates coarse globular spinel and hafnia grains and pores of different size instead (see Figure 8). The growth of the TGO does not follow a parabolic or sub-parabolic growth rate relationship of the no-Hf-containing TBC systems, but rather an approximate growth behavior somewhere in a parabolic and linear buildup of thickness with time. The obvious mass flow control over the oxidation process no longer depends on the alumina matrix alone, but also on the other phases of spinel and hafnia, which are non-protective.

The inward-directed oxide growth *via* cation-ruled transport processes at the metal/TGO interface has been replaced by an anion-dominated transport process accounting for the outward directed diffusion of Al, Ni, Cr, Co, and Hf precipitating as spinel phases and hafnia in a variety of shapes within a porous alumina matrix (see Figure 8). The inherent porosity in the TGO below the mixed zone is indicative for the accumulation of back-diffusing vacancies.

The accumulating Y + Zr content (at pct) in the mixed zone mentioned in Figure 3 *via* cation-ruled transport processes vs the parameter of relative lifetime shows a positive slope. On the other hand, the present Y + Zr content (at pct) in the mixed zone has diminished under anion-dominated transport conditions and has changed to a negative slope vs real lifetime in hours (see Figure 7).

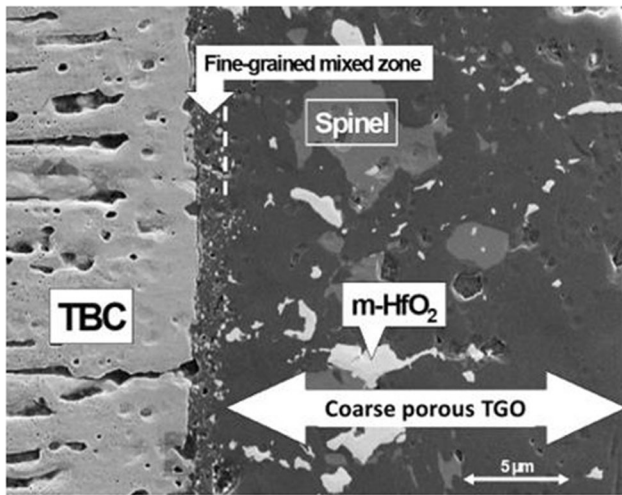


Fig. 8—Cross section through the TBC/TGO zones of a CMSX-4/NiCoCrAlY + Hf/YSZ TBC system at intermediate life (after 2587 hot hours *alias* 3104 cycles at 1100 °C). It displays the TGO being defined by a fine-grained MZ next to the YSZ topcoat and a coarse-grained alumina at the right. The NiCoCrAlY bond coat (not shown here) is co-doped with additional Hf. Reprinted from Ref. [12] under the terms of the CC BY license.

XI. EFFECT OF LOW-CHARGED CATIONS (E.G., Ti^{1+}) ON THE TYPE OF MASS TRANSPORT OF HF-CODOPED NICOCRALY BOND-COATED PRECIPITATION-HARDENING SUBSTRATE ALLOYS

As mentioned before, some cations change their oxidation state as a function of the oxygen partial pressure. For example, Ti has the valences $1+$, $2+$, $3+$, and $4+$. Accordingly, the Ti–O phase diagram shows the phases Ti_2O , TiO , Ti_2O_3 , and TiO_2 , all of which exist continuously up to their melting points.^[15] Therefore, the Ti cations in a low p_{O_2} at the bond coat side of the TGO or at least a certain proportion of them exist most likely as monovalent Ti^+ .

Cation transport in the TGO usually occurs *via* site changes with existing cation vacancies V_{Al}^{ooo} , which are intended for the transport of trivalent cations. If, for example, instead of a trivalent cation a monovalent cation Ti^{1+} enters a vacancy V_{Al}^{ooo} , it turns now into a regular one-charged atom site in the cation sub-lattice. This arrangement, however, contradicts the electro-neutrality condition with respect to equal amounts of positively and negatively charged point defects as given in Eq. [1]. If, on the other hand, an oxygen vacancy V_{O}^{oo} in the anion sub-lattice is removed, then the electro-neutrality condition is satisfied. The given example for a single cation is transferable to similar specific cases of highly Ti-alloyed precipitation-hardening super-alloy system, e.g., the IN100 substrate alloy. Accordingly, the higher the supply of Ti from the substrate, the greater the decrease in the concentration of oxygen vacancies is to be expected. As discussed above, the mass transport of Hf-doped NiCoCrAlY bond-coated solution-hardened substrates is anion-controlled. If, however, the supply of Ti increases, e.g., *via* replacing an existing substrate with a precipitation-hardening

substrate with a high Ti content, the concentration of oxygen vacancies V_{O}^{oo} will drop below a critical value. This event results in a transition from an anion-dominated to a cation-dominated mass transport mechanism. By comparison, cations are the faster moving species. It runs faster, and the lifetimes become shorter.

The lifetimes now correspond to those of similar test objects that have received NiCoCrAlY bond coats without Hf doping. The fracture pattern displaying separation failure at the Me/TGO interface at the end of life is comparable to that of typical cation-ruled failure mode shown in Figure 4.

XII. SUMMARY AND IMPLICATIONS FOR FURTHER RESEARCH

Investigations on zirconium oxide-coated test samples for gas turbines provide a unique approach for examining the RE effect on alumina-forming alloys. These samples form an extraordinary mixed zone below the zirconia thermal barrier topcoat, especially on PVD-produced thermal barrier coating systems. It represents a chemical archive about the life of TBC systems. Its chemical composition is directly related to the adhesion *vs* lifetime determined by FCT measurement.

A comparable investigation for the interpretation of the RE effect for chromia-forming alloys, however, is rather unlikely, since Cr does not form any transient oxides in order to get a corresponding mixed zone (MZ). Only a few analogies when comparing the RE effect on alumina- and chromia-forming alloys can be cited. Above all, the stability of Cr_2O_3 compared to Al_2O_3 has to be questioned in two respects. The ion-binding difference representing the stability of a compound is slightly lower, which can manifest itself in various properties. For example, the trivalence of Cr can be shifted which allows to set up CrO_3 (gas) under the influence of low oxygen pressure or high temperature. This condition favors two opposing processes: unstable oxide growth, which is determined by initiating multiple short-circuit transport processes across the scale, and volatilization of Cr_2O_3 at the scale–gas interface. Moreover, the diffusion rate of Cr cations in chromium oxide is markedly higher compared to that of Al in aluminum oxide as indirectly indicated by the distinct differences in the respective activation activities for oxide growth of only 250 *vs* 382 $kJ\ mol^{-1}$.^[16] This circumstance will maintain the outward oxide growth as well as the cation-dominated mass transport in chromium oxide. The oxide growth front is not at the interior TGO/metal interface but at the TGO/gas interface. For a similar reason, a change of the scale growth mechanism from predominant outward to inward mass transport is doubtful due to the high activation energy of oxygen ion diffusion of 419 $kJ\ mol^{-1}$ standing for the slower moving oxygen ions.^[17]

The relationships between the parabolic oxidation rate constants k_p for alumina-forming Ni–Al alloys as a function of the oxygen potential suggest the existence

of favorable minima of the concentration of point defects for both cation- and oxygen-dominated transport processes as shown in Figure 1. The decrease in defect concentration applies to both. Hence, substantially reduced diffusion rates in the p_{O_2} span between Zr-doped and Hf-doped Ni–Al alloys are likely.

In order to be able to better assess this goal, upcoming research of constitutional phase diagrams introducing convenient RE oxides makes sense. Currently, e.g., the reactive elements used in the bond coats of TBC systems are typically Y + Hf. Practical reasons are often given for this practice. Both elements will oxidize during gas turbine operation. But they will probably not interact with each other because they are stuck to the eutectic characteristic of the Y_2O_3 – HfO_2 system^[18] which indicates the action of repelling forces between the oxide phases.

Alternative oxides having the required grade of chemical stability as well as an outstanding low dissociation pressures are assumed to be offered by pyrochlore compounds, e.g., of the $Hf_2RE_2O_7$ type. This oxide type, however, is a size compound which indicates that its optimal stability depends on the diameter of the ionic radii to be in the right ratio to one another. As the apparent ionic radius of Y^{3+} is too small to interact with Hf no corresponding pyrochlore compound will form. On the other hand, RE is representing the trivalent lanthanides lineup. Although they have very similar chemical Pauling values, they have different ionic radii. Hence, a number of these elements should be able to stabilize the crucial oxide compound. Some of this group are expected to meet the condition of a low dissociation pressures to achieve substantially reduced diffusion rates in the oxide scales.

A useful task of constitutional research would therefore be to find appropriate REs to enable this oxide compound type to be realized. They may result in developing novel RE co-doped bond coats that are no longer Y-doped but have superior oxidation resistance. Correspondingly, the adhesion of such an alumina scale on an alloy that has been doped with a hypothetical compound of two reactive elements ($Hf_2RE_2O_7$?) would be optimal.

ACKNOWLEDGMENTS

This paper took advantage of the many years of collaborative research and intensive discussions with my colleagues at the German Aerospace Center (DLR), Materials Research Institute, Cologne, Germany, in particular with Wolfgang Braue which are gratefully acknowledged.

FUNDING

Open Access funding enabled and organized by Projekt DEAL.

CONFLICT OF INTEREST

The author declares that he has no conflict of interest.

OPEN ACCESS

This article is licensed under a Creative Commons Attribution 4.0 International License, which permits use, sharing, adaptation, distribution and reproduction in any medium or format, as long as you give appropriate credit to the original author(s) and the source, provide a link to the Creative Commons licence, and indicate if changes were made. The images or other third party material in this article are included in the article's Creative Commons licence, unless indicated otherwise in a credit line to the material. If material is not included in the article's Creative Commons licence and your intended use is not permitted by statutory regulation or exceeds the permitted use, you will need to obtain permission directly from the copyright holder. To view a copy of this licence, visit <http://creativecommons.org/licenses/by/4.0/>.

REFERENCES

1. L.B. Pfeil, U.K. Patent No. 459848, 1937.
2. D.P. Whittle and J. Stringer: Improvements of high temperature oxidation resistance by addition of reactive elements or oxide dispersions. *Trans. R. Soc. Lond. A*, 1980, vol. 395, pp. 309–29.
3. J.L. Smialek: Invited paper in commemoration of over 50 years of oxidation of metals: alumina scale adhesion mechanisms: a retrospective assessment. *Oxid. Met.*, 2022, vol. 97, pp. 1–50.
4. P.Y. Hou: The reactive element effect—past, present and future. *Mater. Sci. Forum*, 2011, vol. 696, pp. 39–44.
5. R. Dieckmann: Diffusion in Oxiden und Wachstum in Oxidschichten, in *Aufbau von Oxidschichten und Hochtemperaturwerkstoffen und ihre technische Bedeutung*. A. Rahmel, ed., DGM Oberursel, Germany, 1983, pp. 57–87.
6. R.H. Chang and J.B. Wagner Jr.: Direct current conductivity and iron tracer diffusion in hematite at high temperatures. *J. Am. Ceram. Soc.*, 1972, vol. 55, pp. 211–13.
7. Kazutomo Hoshino and N.L. Petersen, Cation Self-Diffusion in Cr_2O_3 , Communications of the American Ceramic Society, 1983, pp. C202–C203.
8. C.A. Barrett: Effect of 0.1 at.% zirconium on the cyclic oxidation resistance of β -NiAl. *Oxid. Met.*, 1988, vol. 30, pp. 361–89.
9. N.M. Yanar, G.M. Kim, F.S. Petit, and G.H. Meier: Degradation of EBPVD YSZ Thermal Barrier Coatings on Platinum Aluminide and NiCoCrAlY Bond Coats During High Temperature Exposure, Proc. Turbine Forum of Technology, *Advanced Coatings for High Temperatures*, Section 14, Dorsten, Germany, April 2002.
10. M.W. Brumm and H.J. Grabke: The oxidation behaviour of NiAl-I. Phase transformations in the alumina scale during oxidation of NiAl and NiAl–Cr alloys. *Corr. Sci.*, 1992, vol. 33, pp. 1677–90.
11. K. Bedu-Amissah, J.M. Rickman, H.M. Chan and M.P. Harmer: Grain-boundary diffusion of Cr in pure and Y-doped alumina. *J. Am. Ceram. Soc.*, 2007, vol. 90, pp. 1551–55.
12. K. Fritscher: The mechanisms of controlling FCT life and failure mode of Ni-based EBPVD YSZ thermal barrier coatings via the effects of both substrate elements and reactive elements doping. *SN Appl. Sci.*, 2020, vol. 2, p. 2158.
13. Ch. Wang, M. Zinkewich, and F. Aldinger: On the thermodynamic modeling of the Zr–O system. *Comput. Coupling Phase Diag. Thermochem.*, 2004, vol. 28, pp. 281–92.

14. B.A. Pint and L.W. Hobbs: The oxidation behavior of Y₂O₃-dispersed β -NiAl. *Oxid. Met.*, 2004, vol. 61, pp. 273–93.
15. G. Welsch and A.I. Kahveci: *Oxidation Behavior of Titanium Aluminide Alloys, Oxidation of High-Temperature Intermetallics*, The Minerals Metals and Materials Society, Warrendale, 1989, pp. 207–18.
16. K.P. Lillerud and P. Kofstad: On high temperature oxidation of chromium. *J. Electrochem. Soc.*, 1980, vol. 127, pp. 2397–2419.
17. B. Burton and G.L. Reynolds: The estimation of the diffusion coefficient of oxygen in Cr₂O₃ from creep measurements. *J. Mater. Sci.*, 1978, vol. 13, pp. 219–21.
18. F.M. Spiridinov, L.N. Komissarova, A.G. Kocharov, and V.I. Spitsyn: The HfO₂-Y₂O₃ system. *Russ. J. Inorg. Chem.*, 1969, vol. 14, p. 1332.
19. G. Santoro, D.L. Deadmore and C.E. Lowell: Oxidation of alloys in nickel-aluminum system with third element additions of chromium, silicon, or titanium at 1100 °C, NASA TN D-6414, 1971.
20. B.A. Pint, B.A. Nagaraj, and M.A. Rosenzweig: Evaluation of TBC-coated β -NiAl substrates without a bond coat, in *High Temperature Coatings II*. N. Dahorte, J.M. Hampikian, and J.J. Stiglich, eds., The Minerals Metals and Materials Society, Warrendale, 1996, pp. 163–74.
21. P. Saltykov, O. Fabrichnaya, J. Goczewski, and F. Aldinger: Thermodynamic modeling of oxidation of Al-Cr-Ni alloys. *J. Alloys Compd.*, 2004, vol. 381, pp. 99–113.
22. J. Balmain and A.M. Huntz: Improvement of the application of an electrochemical method for the determination of transport properties of an α -alumina scale. Part II: Influence of yttrium and palladium on alumina scales developed on a β -NiAl alloy. *Oxid. Met.*, 1996, vol. 46, pp. 213–34.
23. M.J. Stiger, N.M. Yanar, M.G. Topping, F.S. Pettit, and G.H. Meier: Thermal barrier coatings for the 21st century. *Int. J. Mater. Res. Adv. Tech.*, 1999, vol. 90, pp. 1969–78.
24. I. Barin, O. Knacke, and O. Kubaschewski: *Thermochemical Properties of Inorganic Substances*. Springer, Berlin, 1977.
25. K. Fritscher, C.J. Kröder, and U. Schulz: Adherence and failure of an EBPVD 7YSZ coating on a β/γ -NiCrAl substrate: a pilot study. *Oxid. Met.*, 2016, vol. 86, pp. 279–98.
26. W. Braue: Phase relationships and defect structure during oxide formation and growth in NiCoCrAlY- and (Ni,Pt)Al-based TBC system, in 2005 *Gordon Research Conference on High-Temperature Corrosion*, Colby Sawyer College, New London, NH, July 24–29, 2005.
27. M. Bartsch, B. Baufeld, S. Dalkılıç, I. Mircea, K. Lambrinou, L. Leist, J. Yan, and A.M. Karlsson: Time-economic lifetime assessment for high performance thermal barrier coating systems. *Key Eng. Mater.*, 2007, vol. 333, pp. 147–54.
28. K. Fritscher: Life and FCT failure of Ytria- and Ceria-stabilized EBPVD on Ni-base substrates. *Oxid. Met.*, 2019, vol. 91, pp. 131–57.

Publisher's Note Springer Nature remains neutral with regard to jurisdictional claims in published maps and institutional affiliations.